Asynchronous Depth Sensing through Direct Time-of-Flight Flash LiDAR

Yiyang Liu, Rongxuan Zhang, Filip Taneski, Istvan Gyongy and Robert K. Henderson
Institute for Integrated Micro and Nano Systems, School of Engineering,
The University of Edinburgh, Edinburgh, UK
Email: Y.Liu-305@sms.ed.ac.uk, R.Zhang-65@sms.ed.ac.uk, filip.taneski@ed.ac.uk,
igyongy2@exseed.ed.ac.uk, robert.henderson@ed.ac.uk

***Abstract*—In this paper, we present a novel asynchronous depth-sensing approach utilizing direct Time-of-Flight (dToF) flash LiDAR technology based on Single Photon Avalanche Diodes (SPAD). Our method introduces an asynchronous peak detection mechanism that continuously monitors histogram formation within each pixel, enabling efficient, latency-minimized depth measurement without the constraints of traditional frame-based systems. An adaptive thresholding technique inspired by the Constant False Alarm Rate (CFAR) method is utilized for robust peak detection against ambient photon noise. Experimental validation demonstrates our method's ability to asynchronously report depth events, providing comparable accuracy to conventional methods with reduced latency and enhanced efficiency. Finally, we have proposed a SPAD receiver architecture that showcases the potential for practical hardware implementation in advanced LiDAR applications.**

***Index Terms*—3D ranging, light detection and ranging(LiDAR), single photon avalanche diode(SPAD), neuromorphic sensing.**

I. INTRODUCTION

Recent advancements in direct time-of-flight (dToF) LiDAR receivers using single-photon avalanche diode (SPAD) technology have significantly enhanced high-precision 3D sensing capabilities. These advancements have accelerated development in fields such as autonomous systems, robotics, and consumer electronics by achieving depth measurement accuracies within sub-centimeter range across distances up to several hundred meters [1][2]. Additionally, the integration of on-chip histogramming, peak detection, and ambient photon mitigation modules has effectively reduced the data output volume [3][4][5][6]. Despite these improvements, the majority of LiDAR systems employ frame-based readout techniques, which involve sensor exposure for a predetermined period before processing and retrieving the frames. This traditional approach encounters difficulties when dealing with complex scenes involving either moving targets or objects with varying depths and reflectivities, resulting in increased latency and reduced photon efficiency.

In recent years, image sensors with event-based readout circuits [7] have increasingly gained attention. These sensors can operate in an asynchronous mode, allowing data output independent of a fixed frame rate. This capability reduces power consumption and minimizes latency. Inspired by previous work on event-based vision sensors, e.g., Time to First Spike (TTFS) [8], Dynamic Vision Sensors (DVS) [9], and SPAD-based neuromorphic vision sensors [10], we have proposed a novel asynchronous peak detection and readout method for dToF flash LiDAR systems [11]. This approach enables asynchronous peak detection and reporting by continuously monitoring histograms within each pixel, as shown in Fig. 1. It is worth noting that in [12], S. Park et al. demonstrated a similar asynchronous peak detection approach but implemented it in a frame-based manner, preventing pixels from being reported if the SNR in the pixel was not higher than the threshold at the end of each frame. In this work, we have demonstrated the proposed method in an indoor LiDAR system based on a 256×128 CMOS SPAD imager [4]. We successfully emulated the asynchronous peak tracking approach by reading out raw histograms every 5 laser cycles from the sensor and reconstructing the histogram formation process through off-chip processing using the proposed asynchronous peak tracking approach.

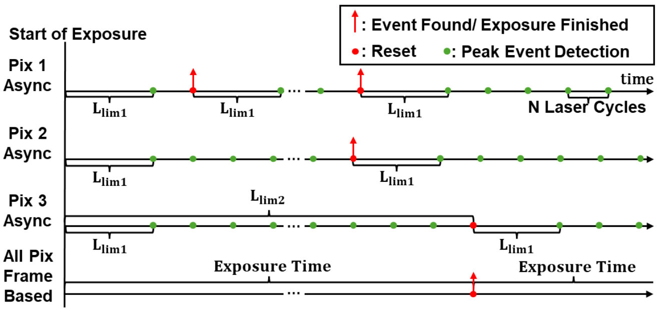

Fig. 1: Pixel operation of the proposed asynchronous LiDAR receiver.

II. ASYNCHRONOUS PIXEL OPERATION

A. Overall Operation

The operational principle of the proposed asynchronous LiDAR system is illustrated in Fig. 1 and Fig. 2. In these figures, L_{lim1} and L_{lim2} represent the minimum and maximum allowable numbers of laser cycles since the last detected peak, respectively. These parameters serve to prevent premature firing before adequate histogram formation and to mitigate delayed firing due to the saturation of histogram bin counters.

This work is funded by EPSRC EP/S026428/1

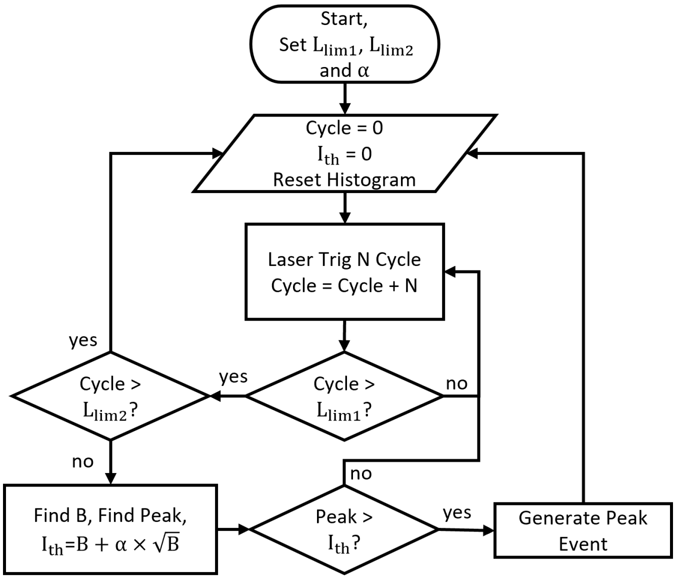

Fig. 2: Pixel operation flow chart.

The parameter α is a constant used for threshold control, which will be further discussed in Section II-B. The variable $Cycle$ denotes the number of laser cycles since the previous firing, while I_{th} represents the peak event threshold.

B. Adaptive Peak Thresholding

To determine an appropriate threshold for peak event detection, an adaptive thresholding approach inspired by the Constant False Alarm Rate (CFAR) algorithm [13] is employed. In a LiDAR system utilizing a multi-event Time-to-Digital Converter (TDC), most histogram bins correspond to the photon level of the ambient background, which is assumed to remain constant across the histogram. Consequently, the background photon level can be estimated as the average value of histogram bins, given by $B = \bar{H}$.

Since the actual bin counts of the background are influenced by photon shot noise, they are expected to follow a Poisson distribution with a mean λ equal to the expected background count value, i.e., $\mathbb{E}(B)$. Moreover, as the histogram is accumulated over a large number of laser cycles, the distribution of background bin counts can be approximated by a Normal distribution with both mean and variance equal to B, according to the Central Limit Theorem. Based on this, the threshold can be set at $\alpha\sigma$ above the background mean, leading to the threshold expression: $I_{th} = B + \alpha\sqrt{B}$.

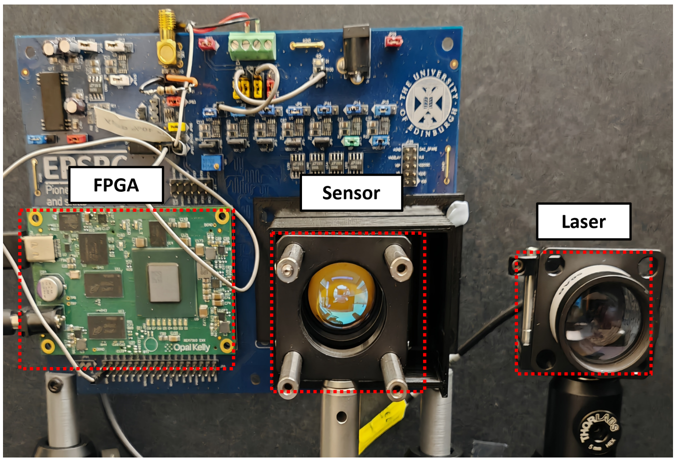

Fig. 4: Experiment setup.

III. EXPERIMENT

A. Experiment Setup

For the purpose of feasibility demonstration, we have used a LiDAR setup shown in Fig. 4. The sensor used in this system contains 256×128 SPADs, with a sliding peak searching algorithm implemented in each 4 by 4 binned macro pixel, where the partial histogram output consists of 8 bins with a TDC resolution of 8.75 ns [4]. The sensor is controlled by Opal Kelly XEM6310 FPGA that is also used to generate the 1.2 MHz, 1.2% duty cycle triggering signal for the OSELA 860 nm TOFI laser module, which has a peak power of 2 W.

Since the sensor in the system reports in frames, it is not possible to implement the proposed method directly on the

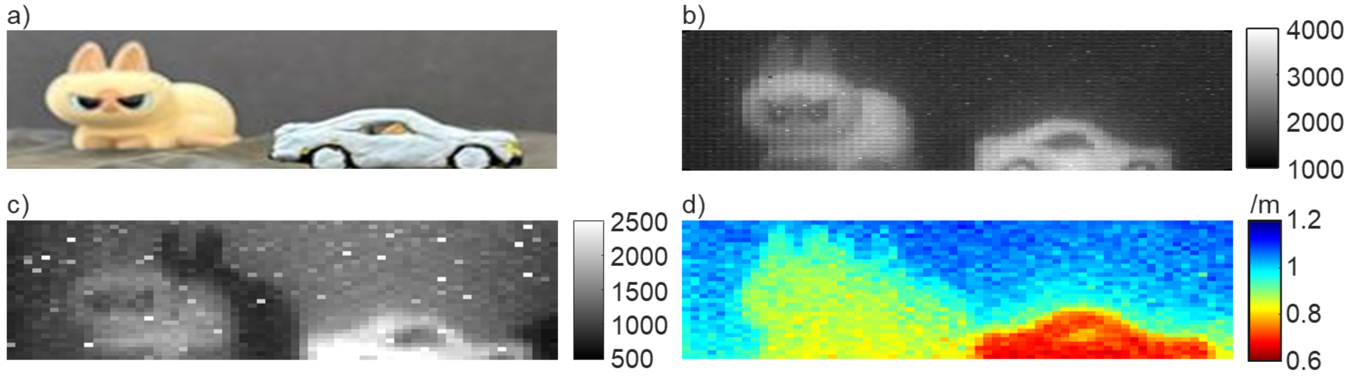

Fig. 3: Images of the scene, a) RGB; b) passive photon counting image with Laser off; c) active photon counting image with Laser on and filter on; d) depth map from the frame-based model.

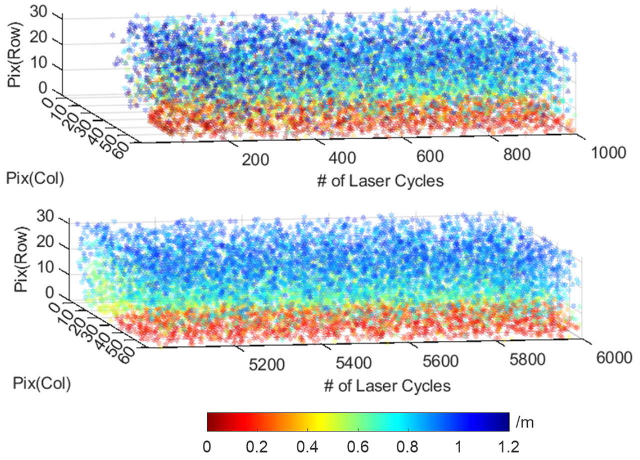

Fig. 5: Spatiotemporal event plot at $\alpha = 8, L_{lim1} = 100, L_{lim2} = 400, N = 2$ for a) Laser cycle 1 to 1000; b) Laser cycle 5001 to 6000.

system. Therefore, the raw partial histogram data is reported from the system every 5 laser cycles, which is the lowest achievable number. Later, the batch of data from every 5 laser cycles was processed offline on a PC to perform peak detection and peak event generation. It is also worth noting that in this work, the sliding peak searching function is not used, as the scene is fixed. Additionally, a Centre-of-Mass Method (CMM) is applied for peak interpolation after identifying the peak bin.

B. Imaging the Scene

In this section, a scene shown in Fig. 3 is used to evaluate the proposed asynchronous method. In this figure, a) shows the RGB image of the scene taken with the RGB camera on iPhone 16; b) and c) are passive and active images of the scene taken in the photon counting mode of the sensor when the laser is off and on, respectively. It is clear that in c), the system creates shadows as the illuminator and receiver are non-coaxial, which also affects the depth measurements. Finally, d) shows the depth map extracted using the frame-based method with exposure of 2000 laser cycles.

The asynchronous method's output is depicted in Fig. 5, showing the spatiotemporal distribution of peak events. Each point in the plot indicates a detected peak event at a specific pixel and time point. The depths reported by peak events are colour coded, where the peak events of the car, the cat, and the background can be approximately found with red, yellow-green, and blue, respectively. This figure demonstrates that peak events are reported asynchronously, validating the feasibility of the proposed method.

To evaluate the quality of the depth reported by the peak events, we first gather the depth values from the final events reported by each pixel, as shown in Fig. 6a). When comparing this to Fig. 3d), it becomes evident that the final depth map produced by the asynchronous method exhibits more noise than the frame-based method. This increased noise arises because this image relies solely on the information obtained from the last peak event. In contrast, Fig. 6b) presents the depth map where the average depth value from all peak events is used for each pixel. This results in a less noisy depth map, making it more comparable to the frame-based method.

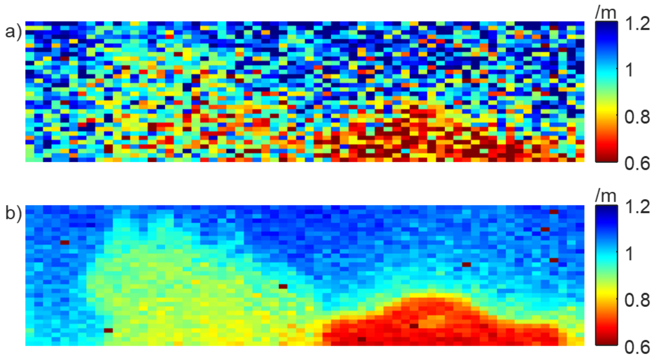

Fig. 6: Depth map reported by the proposed method for a) last event; b) the average of all events.

Fig. 7 displays the counts of the peak events within the 10000 laser cycles of each pixel, highlighting a clear relationship between peak counts, depth, and object reflectivity. Objects closer to the sensor or with higher reflectivity yield higher photon counts per pixel, thus increasing the number of peak events. Additionally, the figure illustrates peak event timing for three different pixels: the car, the cat, and the cat's shadow. It is evident that peak detections for all three pixels occur asynchronously, and the frequency of event reporting correlates directly to the laser signal strength at each pixel, as shown in Fig. 3(c).

In LiDAR systems, in addition to depth information, it is

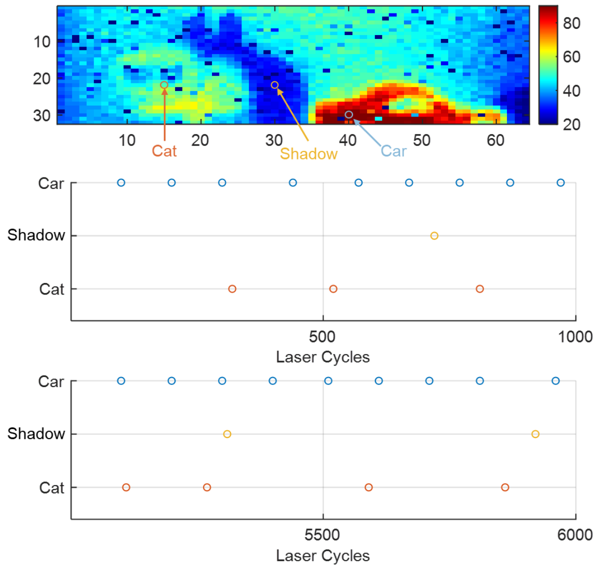

Fig. 7: Counts of the peak events and the event firing status of pixels correspond to different objects.

also important to report the relative reflectivity of objects, ρ, which is typically obtained using the equation $\rho = P_{rx} \times z^2$. Since the received laser photon count, P_{rx}, is directly proportional to ρ and inversely proportional to the square of the object depth, z^2 [14], the reflectivity can be inferred accordingly. In the proposed asynchronous method, P_{rx} is replaced with the number of peak event counts, as shown in Fig. 7. The reconstructed normalized reflectivity is presented in Fig. 8.

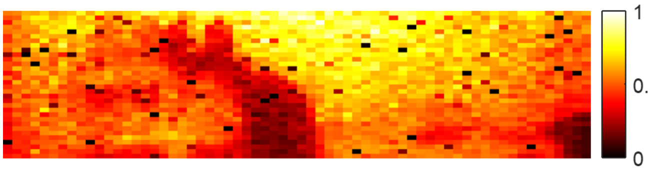

Fig. 8: Reconstructed normalised reflectivity.

C. Hyperparameters Exploration

As stated in Section II-B, the hyperparameters α, L_{lim1}, L_{lim2}, and N must be determined manually before the process begins. Among these parameters, N and L_{lim2} are defined for resource sharing and restart mechanisms to prevent pixel overruns, respectively. These two parameters have a limited impact on system accuracy.

Therefore, in this section, a flat board positioned at a distance of 1.15 m is imaged. By varying the Signal-to-Background Ratio (SBR), α, and L_{lim1}, the False Detection Rate (FDR) and Root Mean Square Error (RMSE) of the detected peak events for all pixels over 10,000 laser cycles are recorded, as shown in Fig. 9. In this plot, a false detection is defined as any detection occurring outside of ±1 bin of the histogram after CMM interpolation, and the RMSE is calculated between the peak events and the ground truth of the distance.

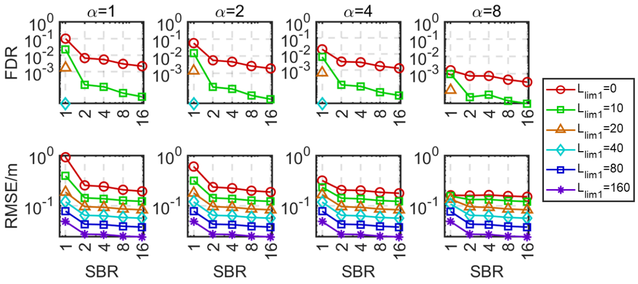

Fig. 9: FDR and RMSE with varying α and L_{lim1}.

It is possible to find in this graph that the increment of both α and L_{lim1} will lead to decreased FDR and RMSE. It is also evident that α has more impact on the lower level of SBR and L_{lim1}, this is foreseeable since it is just controlling the σ level for threshold. On the other hand, the value of L_{lim1} affects the FDR and RMSE level under all conditions, but however increasing L_{lim1} will lead to an increment in the latency as it introduces an increased number of laser cycles after each event report. In the extreme condition that $L_{lim1} \rightarrow L_{lim2}$, the system operates identically to the conventional frame-based LiDAR system.

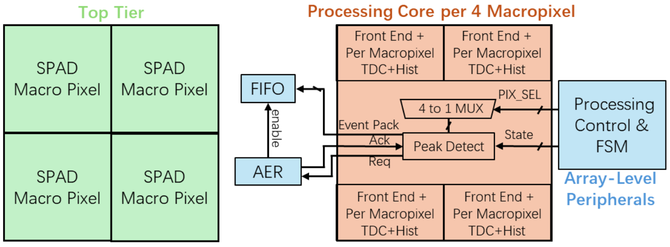

Fig. 10: Block implementation of the proposed method in a pixel array.

IV. PROPOSED CHIP ARCHITECTURE

The potential hardware implementation is shown in Fig. 10. In the proposed implementation, in the top tier, the SPADs are combined into macro pixels through binning. And in the bottom tier, except for the essential SPAD front-end, TDC, and Histogram modules, the rest of the area is used to form a processing element for these 4 pixels. The histogram of the pixels will be transmitted to the processing block alternatively, which is equivalent to $N = 4$ for each pixel. This block will then detect the peak concurrently with the exposure, ensuring that no latency will be introduced by the processing block. Finally, it will send a REQ handshake signal to read out the AER blocks if the peak event is detected. A more detailed demonstration of this implementation on FPGA can be found in [11].

V. CONCLUSION

This paper proposed and validated an asynchronous peak detection and readout method for Time-of-Flight LiDAR systems using CMOS SPAD imagers. The method reduces latency, improves photon efficiency, and accurately retrieves depth by averaging multiple asynchronous events. Experimental results and hardware implementation demonstrate its feasibility for real-time, high-precision 3D sensing in future LiDAR systems.

REFERENCES

[1] C. Zou et al., *ISSCC*, 2024.
[2] O. Kumagai et al., *ISSCC*, 2021.
[3] C. Zhang et al., *IEEE JSSC*, 2019.
[4] I. Gyongy et al., *IEEE JSTQE*, 2024.
[5] S. Park et al., *IEEE JSSC*, 2022.
[6] D. Stoppa et al., *IISW*, 2021.
[7] K. Boahen, *IEEE TCAS-II*, 2000.
[8] S. Chen et al., *ASSCC*, 2005.
[9] P. Lichtsteiner et al., *IEEE JSSC*, 2008.
[10] R. Gomez-Merchan et al., *ESSCIRC*, 2023.
[11] Y. Liu et al., *ISCAS*, 2025.
[12] S. Park et al., *ISSCC*, 2025.
[13] A. Coluccia et al., *MDPI Sensors*, 2020.
[14] A. Tontini et al., *MDPI Sensors*, 2020.